MTLA 40 (2025) 102402

Contents lists available at ScienceDirect

Materialia

journal homepage: www.elsevier.com/locate/mtla

# Development and characterization of silk fibroin-enriched 3D printed hydrogels for photosensitizer delivery

Jose Eduardo U. Rojas [a,b], Lídia Maria de Andrade [c], Wendel A. Alves [b], Francesca Giuntini [a,*]

[a] School of Pharmacy and Biomolecular Sciences, Byrom Street Campus, Liverpool John Moores University, Liverpool, L3 3AF, UK
[b] Center for Natural and Human Sciences, Federal University of ABC, 09210-580, Santo André, SP, Brazil
[c] Department of Physics, ICEx, UFMG, Avenida Antonio Carlos 6627, 31270-901, Belo Horizonte, MG, Brazil

ARTICLE INFO

*Keywords:*
Photodynamic therapy
3D printed hydrogels
Silk fibroin
Photosensitizer delivery
Biocompatible polymers

ABSTRACT

Photodynamic therapy (PDT) uses photosensitizing drugs and visible light to produce cytotoxic reactive oxygen species for targeting cell death. The aggregation of photosensitizers poses a significant challenge to the delivery of the treatment deeper within the tissue. In this study we developed 3D-printed hydrogels composed of gelatin/alginate and Pluronic® F127/alginate polymers with various silk fibroin concentrations to act as reservoirs for the sustained delivery of photosensitizers using water-soluble porphyrin and phenalenone as model drugs. We used rheology and spectrophotometry to analyze the 3D hydrogel scaffolds, focusing on the effect of silk fibroin on photosensitiser incorporation and release. The study showed that increased silk fibroin concentration affected the mechanical strength and the printability of the hydrogels. Compression analysis showed decreased hydrogel mechanical strength at higher silk fibroin concentrations, and cell viability assays indicated the biocompatibility of these hydrogels. Rapid photosensitizer release was observed, aligning with first-order kinetics for gelatin-based and the Higuchi model for hydrogels based on Pluronic® F-127. These findings highlight the potential of 3D-printed hydrogels as a reservoir for the sustained release of photosensitizers and underscore the importance of hydrogel formulation.

## 1. Introduction

Photodynamic therapy (PDT) is a therapeutic approach that attracted attention thanks to its potential to treat ailments such as cancer, microbial infections, age-related macular degeneration, and pre-malignant conditions in a selective and minimally invasive fashion [1]. PDT destroys the target cells through the simultaneous presence of a photosensitizing agent, visible light, and molecular oxygen. Following the absorption of light by the photosensitizers, energy (Type II) or electrons (Type I) are transferred from the excited photosensitizer to molecular oxygen, resulting in the generation of reactive oxygen species (ROS), responsible for causing oxidative damage to biomacromolecules in the vicinity of the photosensitizer, and ultimately leading to the death of the cell [2]. The individual elements of PDT are virtually non-toxic, and their co-localization in the target cells is the key to the selectivity of the treatment and its ability to leave nearby healthy tissues unharmed. The possibility of delivering the treatment with few side effects, especially compared to chemotherapy and radiotherapy, and the applicability in outpatient settings made PDT an extremely attractive approach against cancer [3]. In parallel, the comparative ease of performing light irradiation on the surface of tissues rather than within them steered many applications of PDT toward treating malignant and non-malignant affections of the skin and hollow organs [4].

Delivering therapeutic agents through the skin or the mucosae presents significant challenges. This is particularly true for the skin, whose primary function is to create a protective barrier against external agents, including toxins and pathogens. The structure of the *stratum corneum*, the outermost layer of the skin, restricts the permeation of large and/or hydrophilic molecules, preventing most therapeutic agents from reaching the inner layers of the skin and the deeper tissues. Most photosensitizers display a high molecular weight and hydro-lipophilic features that exacerbate the challenges to skin penetration. The chromophore, responsible for the absorption of light that triggers the photodynamic process, is often lipophilic, limiting the applicability of the water-based formulations commonly used in topical delivery systems [5]. Chemical modifications aimed at achieving a favorable

* Corresponding author.
*E-mail address:* F.Giuntini@ljmu.ac.uk (F. Giuntini).

https://doi.org/10.1016/j.mtla.2025.102402
Received 28 November 2024; Accepted 31 March 2025
Available online 1 April 2025

hydro-lipophilic balance for optimal skin penetration may afford species that aggregate in water, a behavior that reduces photodynamic efficiency [6]. Overcoming these challenges inspired the exploration of different approaches to enhance the penetration of photosensitizers in the skin, including micellar systems, lipid-based formulations [7], hydrogels [8], and transdermal drug delivery systems relying on physical or mechanical methods, such as microneedles [9], ultrasound, or electroporation [10,11], Most of these approaches, focused on enhancing the effectiveness of phototherapy by mitigating its adverse effects on the surrounding tissues and enabling control of the timing and dosage of light exposure [12].

Our group recently focused on the potential of soft materials containing *Bombyx mori* silk fibroin (SF) as a reservoir for the transdermal delivery of porphyrin photosensitizers [13]. SF attracted considerable interest as a material for biomedical applications due to its high biocompatibility, low allergenic potential, tunable degradation rate, capacity to form stable hydrogels, and ease of chemical modification [14]. Thanks to the prevalence of $\beta$-sheet forming regions in its sequence and to its hydrophobicity, SF self-assembles to give materials with favorable mechanical properties, amenable to different fabrication approaches, including electrospinning, spin-casting, electro-spraying, and freeze-drying [15]. SF is particularly suited for PDT applications due to its inherent optical transparency, facilitating effective light penetration for activating photosensitizers [16]. By utilizing SF hydrogels as carriers for therapeutic agents, the controlled release of these agents at application sites becomes possible, thereby promoting the selectivity of the treatment and reducing damage to the surrounding tissues.

In this work, we describe novel photosensitizer-containing 3D-printed scaffolds obtained using combinations of gelatin/alginate or Pluronic® F-127/alginate and varying concentrations of SF. Our results show that the formulation of the ink and the printing parameter plays a significant role in achieving the desired mechanical strength and favorable release profile of photosensitizer molecules. Our findings demonstrate that the presence of silk fibroin markedly influences the properties of the resulting structures, highlighting the importance of fine-tuning the ink composition to achieve the desired photosensitizer release profile and, ultimately, the efficiency of the photodynamic treatment and the therapeutic outcome.

## 2. Materials and methods

### 2.1. Materials

All reagents used in this study were of analytical grade. Silk fibroin was extracted from frisson extra silk (residues from silk processing), provided by Bratac (Londrina, Brazil). Sodium carbonate, lithium bromide, polyethylene glycol (average MW 6000, hereafter PEG-6000), Pluronic® F-127 (hereafter, PL127) and 1H-phenalen-1-one (hereafter, phenalenone) were purchased from Sigma-Aldrich (UK) and were used as received. Gelatin from bovine skin (gel strength 225 g Bloom, Type B) and alginic acid sodium salt were from Sigma (UK) and Acros Organic (UK), respectively, and were used as received. 5,10,15,20-*tetrakis*-(4-sulfonatophenyl)porphyrin tetrasodium was synthesized following literature procedures [17]. Ultrapure water (18.2 MΩ-cm) was obtained from a Millipore Purification System. Cellulose dialysis membrane tubing 12 kDa MWCO and 3.5 kDa MWCO (Sigma Aldrich, UK) were used for the dialysis procedures. 3D printing was performed on a BIO X® Cellink bioprinter using printing parameter detailed below.

### 2.2. Silk fibroin solution preparation

*Bombyx mori* fibroin was isolated by a procedure previously described [13], which was adapted from Rockwood et al[18]. Briefly, 10 g of raw silk was degummed by soaking in aqueous 20 mM (1 L) $Na_2CO_3$ at 85 °C for 60 min to separate the sericin from the fibers. The degummed fibers were rinsed in deionized water for 30 min (3 times) and dried for 24 h at 72 °C. The fibers were dissolved in 9.3 M aqueous LiBr by heating at 80 °C–100 °C on a hot plate with constant stirring to aid in the dispersion of the fibroin. The solutions obtained were purified by dialysis against water for 48 h to eliminate the salts and then were centrifuged to eliminate solid residues. The fibroin solution was further dialyzed using a 3.5 kDa MWCO dialysis tube against 10 % w/v aqueous PEG 6000 until a concentration of 7 % w/v was attained. The fibroin concentration was determined by measuring the residual mass after drying at 37 °C using Eq. (1):

$$SFS\ concentration\ \% = (W_2 - W)/(W_1 - W) \times 100 \quad (1)$$

where: W and $W_1$ represent the plate mass before and after adding 1 mL of silk fibroin solution, and $W_2$ indicates the plate weight after the solution was dried at 60 °C for 4 h. The purified SF solution was stored at 4 °C until use and proved stable in this condition (no visible alteration) for up to 2 months.

**Table 1**
Printing parameters for hydrogels prepared with either gelatin (15 %)/alginate (2 %) or PL127 (30 %)/alginate (2 %) as the base.

| Ink | Gauge (mm) | Pressure (Pa) | Speed (mm/s) | Temperature ( °C) |
|---|---|---|---|---|
| PL127 | 0.41 | 200 | 2 | 25 |
| Gelatin | 0.64 | 60–70 | 2 | 40 |

### 2.3. Ink preparation

Bioinks with different concentrations of SF (0 %, 2 %, 4 %, 6 %) were formulated, using sodium alginate (2 % w/v) as the cross-linking agent and either gelatin (15 % w/v) or PL127 (30 % w/v) as viscosity agents to improve the mechanical properties and printability of the hydrogels. In a typical preparation, 0.1 g of sodium alginate was dissolved in 5 mL of 7 % w/v aqueous SF at room temperature under stirring. For the SF/alginate/gelatin ink, 0.75 g of gelatin was added to the mixture of alginate and SF at 40 °C to maintain the ink in a liquid state. For the SF/alginate/PL127 ink, 1.5 g PL127 was added at 4 °C. Both inks were stored at 4 °C until used. Photosensitizer-containing ink formulations were obtained following a similar protocol, adding the necessary amount of photosensitizer during the process to a final concentration of 1 mg/mL within the hydrogel matrix.

### 2.4. Rheological properties

The viscoelastic properties of the hydrogels were analyzed using a controlled-stress Malvern Ki nexus Lab + rheometer equipped with a parallel plate geometry and a sample gap of 0.1 mm at room temperature. A constant shear stress of 1 Pa was selected to perform the frequency sweep from 0.1 to 20 Hz (0.62–124 rad/s), and the storage(G') and loss (G") moduli were recorded. For the temperature ramp (0 °C −40 °C) experiments, a fixed frequency of 1 Hz (6.28 rad/s) was used.

### 2.5. 3D printing process and printability assessment

The ink was transferred into a 4 mL syringe with a stainless-steel nozzle, which was mounted on a pneumatic print head in the bioprinter. Table 1 details the parameters used for printing the inks containing gelatin or PL127.

A two-layer 10 mm x 10 mm x 1 mm square geometry with a grid filament thickness of 1 mm and a 25 % infill was chosen as a model scaffold for the 3D printing. The scaffold design and the g code file were obtained using the CELLINK proprietary software HeartOS 2.4.4. Upon printing completion, the scaffold was soaked in a 2 % (w/v) calcium chloride solution for 5 min to promote cross-linking. The scaffolds were used after preparation or stored at 4 °C until used for up to one week.

### 2.6. Printing fidelity assessment

To assess the fidelity of various bioinks developed in this study, we printed a simple square design and examined the accuracy of several geometric parameters. Bright-field microscopy images were acquired (1.5X and 43X magnifications), and the printing fidelity was assessed using ImageJ (National Institutes of Health, USA). The filament uniformity and the printing fidelity were calculated using the following equations as parameters to study the printing fidelity of the 3D-printed scaffolds:

$$Filament\ uniformity = \frac{Printed\ strand\ length}{Designed\ strand\ length} \quad (2)$$

$$Printing\ fidelity = \frac{Printed\ area}{Designed\ area}\ x100 \quad (3)$$

Printing fidelity is defined as the degree to which the 3D-printed construct matches the geometry in terms of length and width of the original design file [19].

### 2.7. Fourier transform infrared spectroscopy

FTIR spectra were recorded using a Spectrum Two FTIR spectrometer (Perkin Elmer, UK) in absorbance mode in the 400−4000 $cm^{-1}$ frequency range.

### 2.8. Scanning electron microscopy

SEM images were acquired using an FEI Inspect F50 scanning electron microscope. Each scaffold was sputter-coated with 15 nm of gold, and the images were produced using secondary electrons, 10 kV voltage, and 4 mm spot size.

### 2.9. Swelling and degradation analyses

The stability and swelling properties of hydrogels were tested. Samples of each print type ($N = 3$ per group) were weighted and added to 10 mL of PBS (pH 7.4) and gently shaken in a water bath at 37 °C for 24 h. The hydrogels were removed from the bath, rinsed with deionized water, blotted dry with filter paper to remove surface moisture, and weighed ($W_1$) to determine the swelling ratio using Eq. (4).

$$Swelling\ ratio = \frac{w_1 - w}{w}\ x\ 100 \quad (4)$$

The samples were dried at 60 °C overnight and weighed again, and the degradation ratio (mass loss) was calculated using Eq. (5).

$$Mass\ loss = \frac{w - w_d}{w}\ x\ 100 \quad (5)$$

where w is the initial dry mass of the scaffolds, $w_1$ is the mass of the scaffolds after swelling, and $w_d$ is the weight after drying overnight at 60 °C.

### 2.10. Compression analyses of the 3D-printed scaffolds

A compression test for the printed structures was performed using a TA.XTplusC Texture Analyzer (Stable Micro Systems). The compression speed was set to 0.1 mm/min with a fixed load cell capacity of 25 N. The compressive modulus of the hydrogel was calculated from the slope of the stress-strain curve in the linear region, which represents the stiffness of the hydrogel under compressive forces.

### 2.11. Photosensitizer release

To evaluate the *in vitro* release profile of two photosensitisers from the 3D prints, samples of the printed scaffolds ($N = 3$) containing photosensitizers were immersed in 5 mL PBS (pH = 7.4) at 37 °C. At different time points (0.5, 1, 2, 3, 4, 5, 6, 7,8, 24, 48, and 72 h), 1 mL of medium was removed from the receiving solution and replaced by an equal volume of fresh PBS buffer, to maintain sink conditions. The concentration of the photosensitive molecules in solution was measured by absorption spectroscopy at $\lambda = 420$ nm for the porphyrin and $\lambda = 360$ nm for the phenalenone. The porphyrin and phenalenone concentrations obtained were calculated using the equation of the regression lines obtained by plotting the absorbance vs. concentration of known solutions (expressed in mg/mL).

$$Phenalenone: y = (28.55 \pm 0.61)x + (0.070 \pm 0.003)$$

$$Porphyrin: y = (120.12 \pm 2.13)x + (0.0019 \pm 0.0013)$$

The points obtained (drug concentration vs. time) were fitted to four different drug release models to analyze the kinetic of the release.

The cumulative drug release from the hydrogel matrix over time is calculated by summing the drug concentration at each time point while accounting for the removal of samples during the experiment. The equation is expressed as:

$$Cumulative\ drug\ release = \sum_{i=1}^{n}\left(C_i\ .V + \sum_{j=i}^{i-1} C_j\ .\ V_s\right) \quad (6)$$

where $C_i$ is the drug concentration in the release medium at a given time *i*, $V$ is the total volume of the release medium, and $V_s$ represents the volume of the sample withdrawn at each sampling time. The second summation term corrects for the cumulative loss of drug due to sampling, ensuring that the total drug released is accurately calculated. This approach is critical for maintaining mass balance in the system, especially in studies where aliquots are periodically removed and replaced with fresh medium.

### 2.12. Cytotoxicity test of the 3D printed hydrogels

The compatibility of the printed hydrogels with cell survival was assessed by Resazurin viability assay (Sigma) on HaCat human keratinocytes. Before the assays, the printed and freeze-dried scaffolds were sterilized with gamma radiation (10 kGy). The cells were incubated in 96 well-plates (TPP) with 100 μL of DMEM high glucose, 5 % FBS culture medium (Gibco) for 24 h at 37 °C with 5 % $CO_2$. Then, the printed scaffolds were immersed in the cell-containing medium and left reacting for 24 h. Afterwards, 10 μL of Resazurin was added in each sample and kept on incubation for 4 h at dark. Triton-100X (Sigma) was used as cell death control. The absorbance was measured at 570 nm (Multskan Go, Thermo).

### 2.13. Statistical analysis

The data were presented as means ± *S*.D. of three independent experiments performed in triplicate. A standard significance level of $p < 0.05$ was used. The analyses were performed with GraphPad Prism 8.0 software (GraphPad Software, Inc., La Jolla, CA, USA) or Origin (Pro) (Version Number 2019, OriginLab Corporation, Northampton, MA, USA).

## 3. Results and discussion

### 3.1. Bioink formulation

The ability of SF to assemble into materials with high strength and toughness makes it highly attractive for biomedical applications, especially those in which mimicry of the mechanical properties of tissues is required [20]. The generation of SF-containing 3D structures by additive manufacture, in particular 3D printing, became the object of investigation in regenerative medicine and wound management because it allows

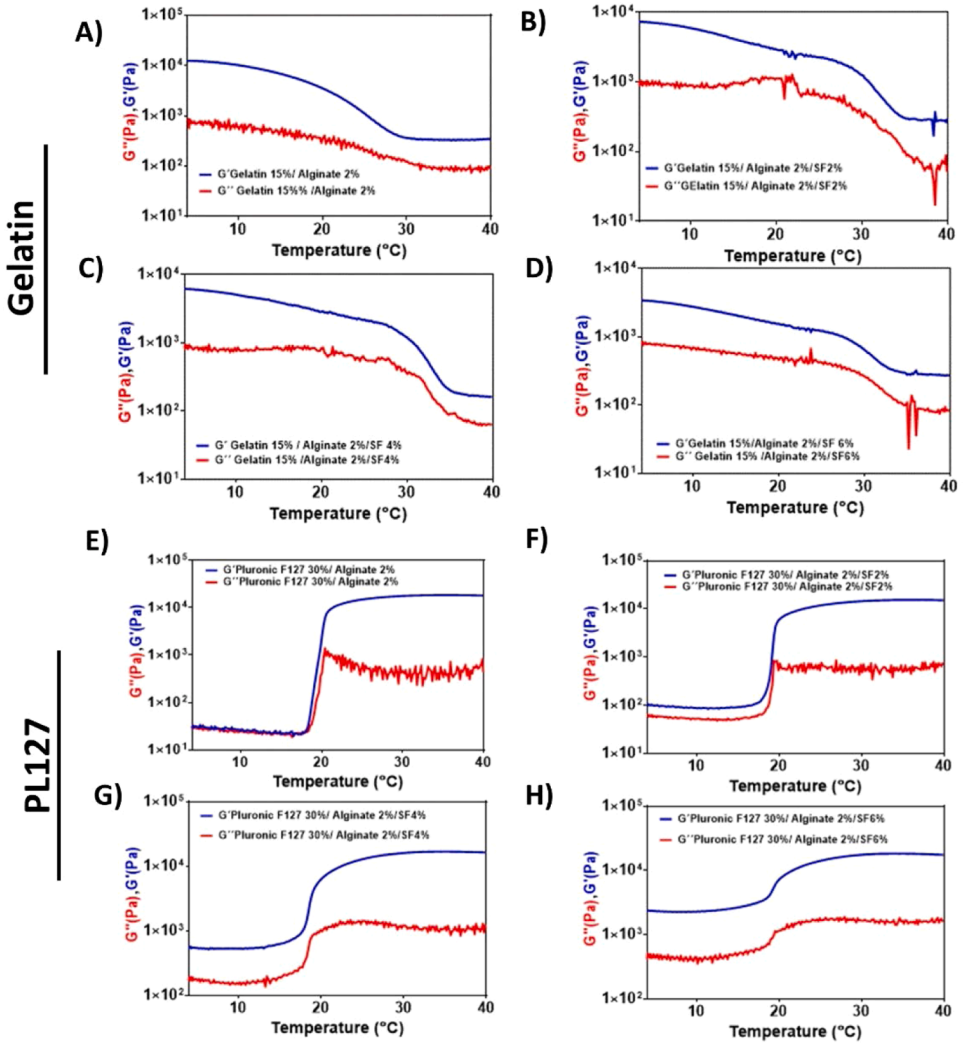


**Fig. 1.** Temperature ramp of hydrogels: A-D) Temperature ramp of gelatin (15 %)/sodium alginate (2 %) hydrogels with different concentrations of silk fibroin for 3D printed scaffolds; E-H) Temperature ramp of PL127 (30 %)/sodium alginate (2 %) hydrogels with different concentrations of silk fibroin for 3D printed scaffolds.

the combination of the extraordinary mechanical features of SF with the fine spatial control of the resulting structure [21,22].

The extraction of SF from *B. mori* cocoons or processed fibers affords SF aqueous solution that can be used to obtain various materials but that do not lend themselves to be used in 3D printing inks because of their low viscosity. One approach to overcome this issue entails the addition of a viscosity enhancer to the SF solution. Biopolymers such as chitosan, gelatin, alginate, or biocompatible synthetic polymers such as PVA or PEG can be used to this effect. The choice of materials that behave as viscosity enhancers and the possibility to vary the composition of the ink to tune both the rheological properties of the ink and the mechanical properties of the printed structure [23–26]. For our study, we chose two viscosity enhancers: PL127 and gelatin.

PL127 is a triblock copolymer composed of poly(ethylene oxide) (PEO) and poly(propylene oxide) (PPO) segments. It exhibits gel transition in the 20–30 °C range *via* a micelle packing mechanism triggered by the aggregation of the PPO blocks. This forms a non-covalent cross-linked network that traps water and other components in a gel-like structure [27]. The sol-gel transition temperature of PL127 solutions is affected by factors such as polymer concentration, molecular weight, and the presence of other compounds in the environment [28,29]. The association of PL127 or other poloxamers has been investigated to obtain nanoparticles or hydrogels [30]. Youn et al. showed that PL127 improved the mechanical properties and reduced the degradation rate of SF-containing hydrogel, enabling control over the release rate of hydrophobic drugs [31].

Gelatin is the product of the hydrolysis of collagen, and it has been widely used in biomedical applications. Its degradability and ability to promote cell attachment made it attractive for decades for drug delivery and tissue repair/regeneration.

### 3.2. *Rheology measurement*

The favorable rheological properties of a hydrogel are fundamental for the success of its application in 3D printing. Shear-thinning behavior is highly desirable to ensure smooth extrusion and shape retention once the filament is deposited on the print bed. Parameters such as yield stress and G' are also crucial to guarantee the integrity of the printed structure upon handling. The rheological properties of hydrogels, which determine their transition between solid-like and liquid-like states, are influenced by factors such as polymer concentration, pH, and temperature [32]. Both gelatin and PL127 hydrogels are known to display a temperature-dependent gelation [33]. Lending themselves to the generation of temperature-responsive inks. In particular, PL127 hydrogels show thermal reversibility, as they liquefy upon cooling and solidify upon heating: this enables the use of temperature as one of the key printing parameters to achieve the desired properties in the printed scaffold [34]. For temperature-responsive inks, the correlation between

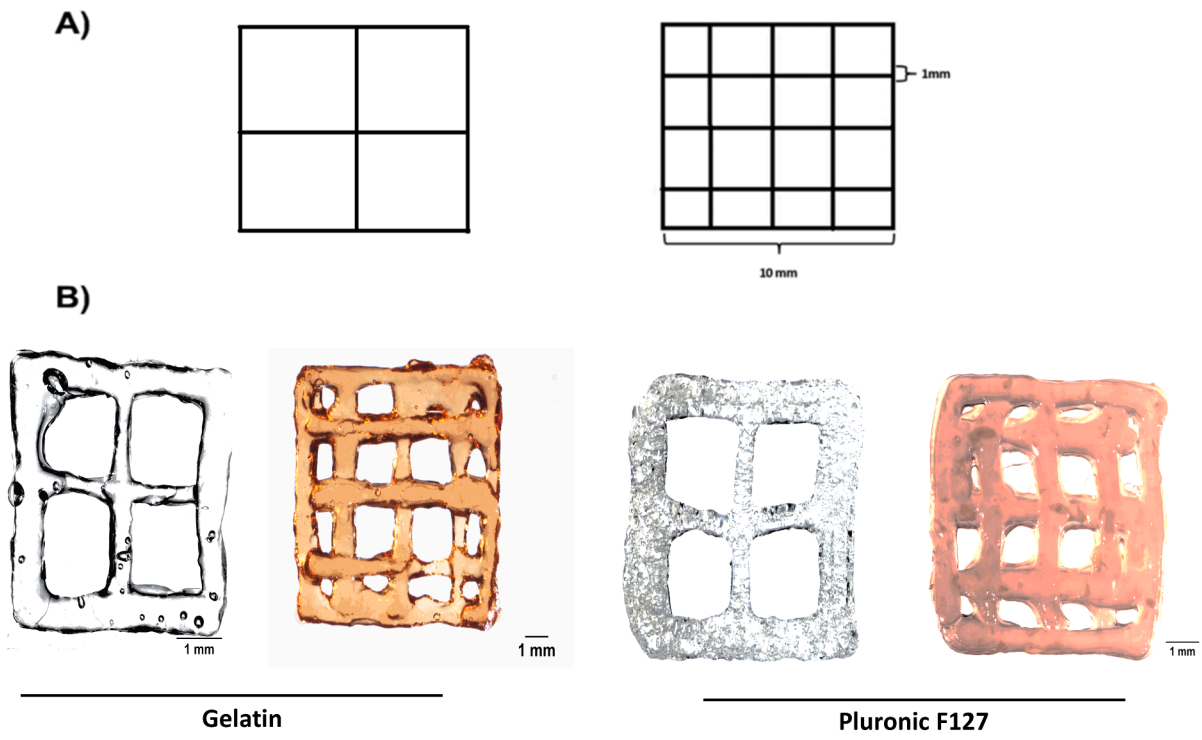


**Fig. 2.** Scaffold design for 3D-printed hydrogels: A) Target shapes of the 3D scaffolds: a square shape with a 10 mm length, made by 1 mm thick filaments; B) Gelatin and Pluronic F127 3D hydrogel scaffolds prototypes.

temperature and hydrogel consistency is a crucial parameter that influences the mechanical properties of the ink during printing. This relationship directly affects the ink's printability, the printed scaffold's shape resolution, and its shape fidelity at the operating temperature. The consistency of the hydrogel ensures that the ink behaves appropriately under different temperatures, which is vital for achieving precise structural outcomes and functional performance in the final application [35]. Judicious formulation of the ink is therefore pivotal to ensure that the temperature gelation range is optimal for the intended application, enabling the use of temperature as a key printing parameter to impart the desired properties in the printed scaffold.

We performed a temperature ramp to analyze the behavior of the storage (G') and loss (G'') moduli of gelatin and PL127 hydrogels to investigate the temperature responsiveness of their gelation (Fig. 1). For all the gelatin-containing hydrogels, G' is higher than G'' throughout the temperature range examined, indicating that the elastic component of the hydrogel dominates (Fig. 1A-D). Although a drop in both G' and G'' values is observed as the temperature increases, indicating a loss of gel strength, the lack of interception between the G' and G'' curves suggests that these measurements were performed below the gel transition temperature. In the absence of SF, the gelatin shows a drop of G' at temperatures between 20 and 30 °C, which aligns with the behavior reported in the literature [34]. The addition of 2 %, 4 %, and 6 % SF to the composition (Figs. 1B-D) causes an increase in the temperature at which the drop in the G' and G'' moduli is observed, indicating that the presence of SF increases the mechanical strength of the formulation. The values of G' observed at lower temperatures decrease with adding SF.

The inks containing PL127 also displayed temperature-sensitive behavior, showing a sharp increase of the G' and G'' values triggered by temperature increase (Figs. 1E-H). Adding a higher percentage of SF in the hydrogel causes a reduction in the magnitude of the increase of both G' and G'' values, without significantly affecting the temperature at which the change is observed. This change affects mostly the value of G' observed at low temperatures, possibly due to increased crosslinking of the hydrogels [36]. As observed for the gelatin-containing hydrogels, no crossover between the G' and G'' values is shown. This behavior suggests that the systems exhibit a degree of cross-linking, preventing the full transition to the liquid state.

We performed a frequency sweep analysis to study the solid-like and liquid-like behavior of the hydrogels in response to mechanical stimuli, as this bears relevance to the suitability of the hydrogels as inks for 3D printing (Figure S1 and S2). The shape of the oscillatory rheology frequency sweep curve can provide insight into the structural and dynamic properties of the material. A material with a high G'-G'' crossover frequency and a broad plateau region in the G' curve indicates a highly cross-linked and structured material. In contrast, a material with a low G'-G'' crossover frequency and a steep slope in the G' curve shows a propensity of the material to a liquid-like behavior and indicates a low degree of cross-linking [37]. Figure S1 shows the frequency sweep curves obtained from the gelatin-containing hydrogels with different concentrations of SF over a shear rate range of $10^{-1}$–$10^{2}$ rad·s$^{-1}$. The *n* and *S* parameters provide a quantitative estimation of the strength of a hydrogel related to its crosslinking density [38]. The G', S, and low n exponent values decrease with increasing SF, indicating that SF decreases the crosslinking density and gives weaker gel structures (Table S1).

The G' values of the PL127-containing hydrogels obtained in this study do not show frequency dependence, indicating a viscoelastic behavior (Figure S2). As observed for the gelatin-containing hydrogels, the G' values of the PL127 hydrogels were higher than the corresponding G'' values throughout the frequency range examined. The addition of SF caused an increase in the G' and S values, indicating the formation of more elastic and crosslinked structures, whereas the low *n* exponent values did not show significant changes (Table S2).

At low frequencies, the material indicates a more viscous flow behavior and shows little resistance to deformation. As the frequency increases, the material behaves more like an elastic solid and exhibits greater resistance to deformation [39,40]. No crossover point was observed between the storage and loss modulus for the tested frequencies, demonstrating that the tested hydrogels possess entangled fibrous networks [41].

Overall, the data show that the presence of silk fibroin alters the

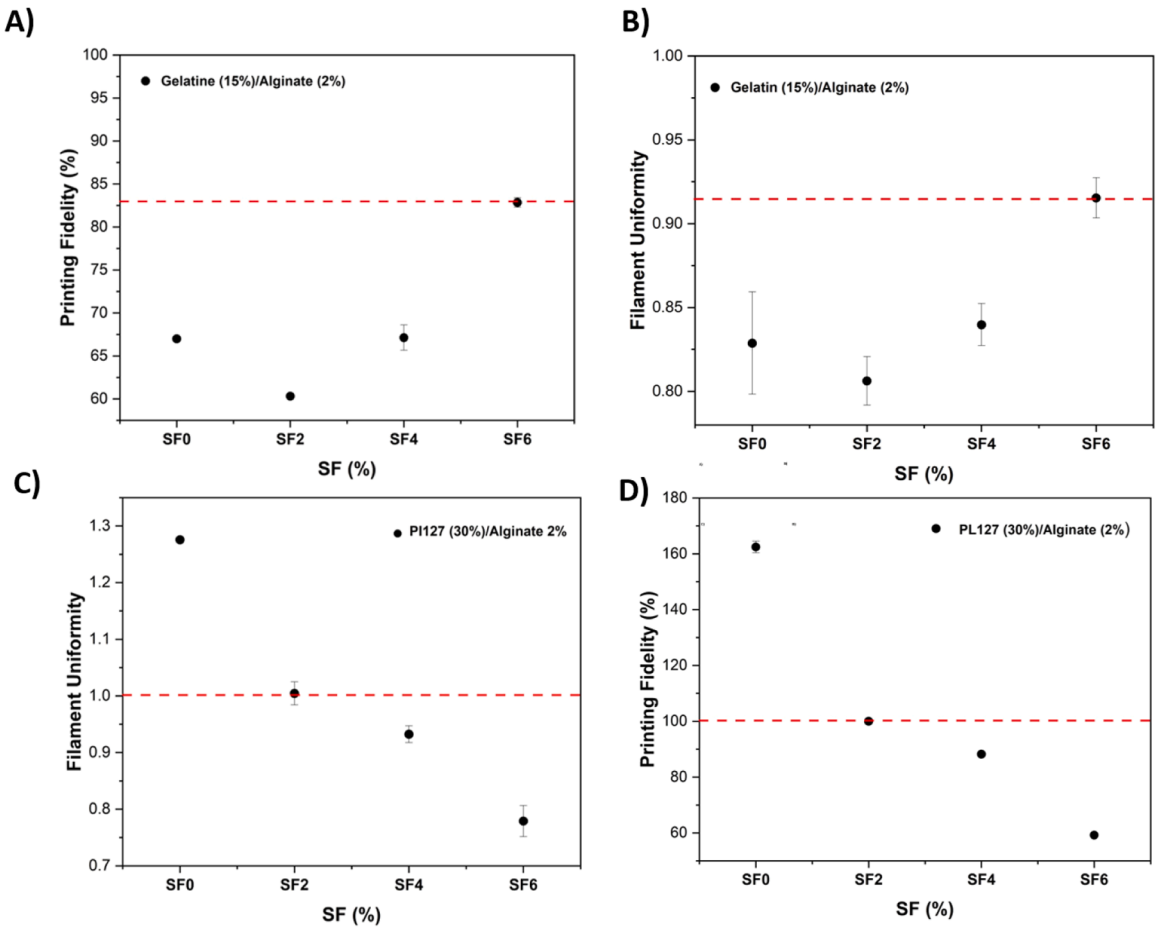


**Fig. 3.** 3D hydrogels printability: A) Filament uniformity of PL137 inks with varying SF concentrations; B) Printing fidelity of PL137 inks with varying SF concentrations; C) Filament uniformity of gelatin inks with varying SF concentrations; D) Printing fidelity of gelatin inks with varying SF concentrations. All inks contain 2 % alginate for cross-linking promoted by calcium ions.

rheological parameters for both gelatin and PL127 hydrogels, as it can affect the temperature at which significant changes in storage/loss moduli are observed and the response of the mixture to mechanical stimuli. Understanding the rheological behavior of these hydrogels can help design and optimize their performance to match the requirements of the intended application [20,42].

### 3.3. 3D printing

In this study, we used extrusion-based printing to prepare the 3D scaffolds. This is a widespread technique, as it is relatively simple and applies to a wide range of hydrogels with different physical and mechanical properties. 3D printing hydrogels allow for the generation of scaffolds with defined customized geometry in a reproducible and expeditious fashion, ensuring the uniform dispersion of bioactive elements and other components throughout the structure.

To perform the initial assessment of ink printability and fidelity to the shape of the structures obtained, we chose the shape of a square (Fig. 2). We reasoned that a simple geometry would be ideal to assess the hydrogel's quality in terms of fidelity to shape during and after printing. The shape can be customized with different infill percentages, allowing grids of different hydrogel densities to be obtained.

The printability of a material refers to its suitability for 3D printing and considers factors such as its flow properties, curing behavior, and adhesion to the printing surface. The printability of hydrogels is influenced by their rheological properties, crosslinking density, and swelling behavior [43,44]. A hydrogel ink suitable for 3D printing must flow smoothly through the printing nozzle but regain viscosity quickly to ensure optimal adhesion to the printing surface, integrity of the printed scaffold, and fidelity to shape [45,46]. Initial optimization of the printing parameters showed that the best results were obtained using the parameters described in Table 1. We first investigated filament uniformity and printing fidelity of the gelatin-containing hydrogels and verified that adding SF benefits both parameters (Figs. 3A and 3B). As we observed previously, increasing the concentration of silk in the ink composition decreases the viscosity of the hydrogel and thus facilitates the extrusion of the ink through the nozzle (Figure S1 and S3A). The hydrogel containing the 6 % SF gave the best results in terms of filament uniformity (> 0.9) and printing fidelity (> 80 %), although it did not allow it to reach the target values of 1 and 100 % the best scaffolds were obtained with this concentration of SF (Figure S4). For the 3D printing of PL127-based hydrogels, we used the parameters described in Table 1. Fig. 3C and D show the printability of the PL137 hydrogels with different concentrations of SF. In line with what the rheological parameters described in the previous section, adding fibroin to the hydrogels increases the G' value of the PL127 hydrogel and its viscosity (Figure S2 and S3B), resulting in a more robust material capable of running smoothly through the nozzle (Figure S4), yet of maintaining its structure after the deposition on the printing surface. The ability of SF to improve the shear thinning behavior and increase the viscosity of the hydrogel, thus facilitating extrusion through the printing nozzle, has been reported [47].

### 3.4. 3D-printed scaffolds characterization

All the 3D printed scaffolds were characterized by scanning electron

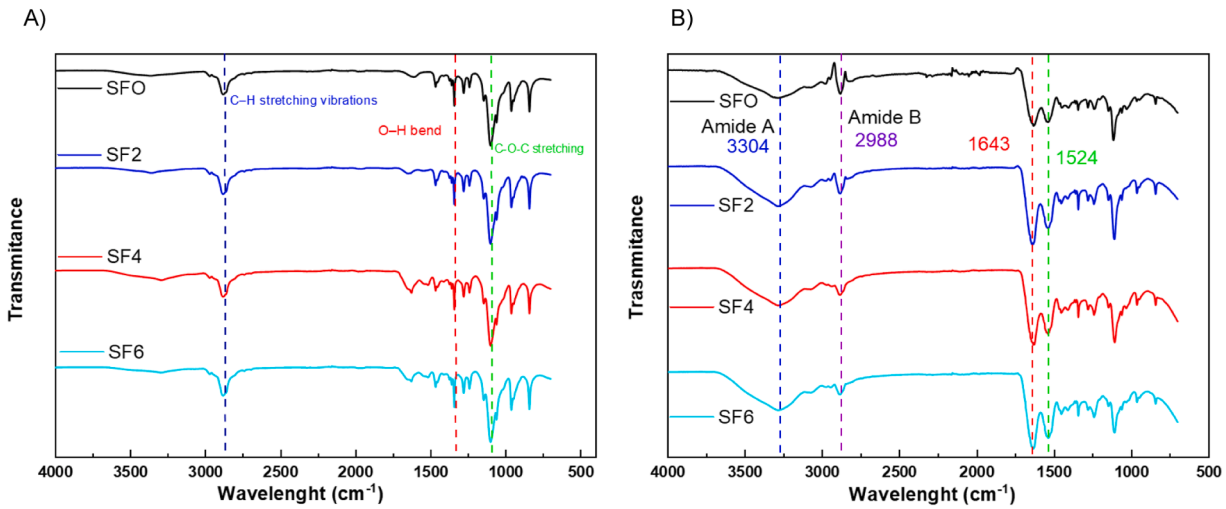


**Fig. 4.** FTIR spectra ( % transmittance vs. wavenumber) of: A) 3D printed scaffolds obtained with PL127-based inks containing different concentrations of SF; B) 3D printed scaffolds obtained with gelatin-based inks containing different concentrations of SF.

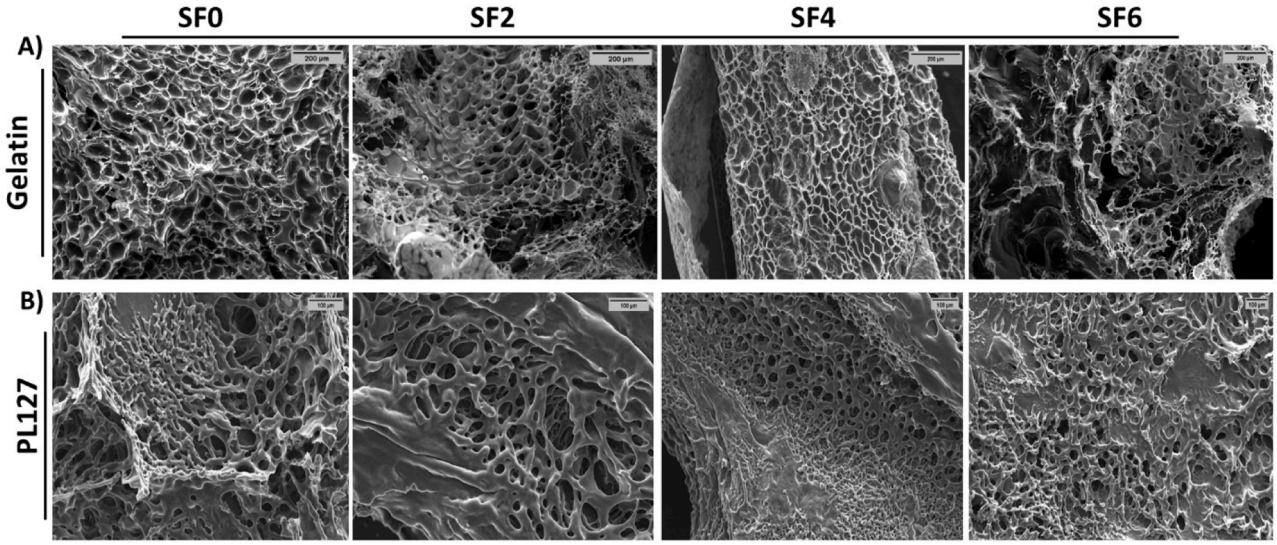


**Fig. 5.** SEM images of the 3D printed hydrogel scaffold: A) Gelatin-containing scaffolds (scale bar 200 μm); B) PL127-containing scaffolds (scale bar 100 μm). SF0: no SF, SF2: 2 % SF, SF4: 4 % SF, and SF6: 6 % SF.

microscopy (SEM) and Fourier transform infrared (FTIR) spectroscopy. Fig. 4 shows the spectra of the gelatin-based scaffolds with different SF concentrations following printing. Several diagnostic peaks are shown in the 4000–600 $cm^{-1}$ spectrum range (Fig. 4A), generated by the functional groups in a protein [48]. Amide A and amide B bands, caused by the N—H and C—H stretching, respectively, appear at ca. 3300 $cm^{-1}$ and ca. 2925 $cm^{-1}$ [49,50]. The peak generated by the peptide backbone amide C═O stretching is visible at ca. 1650 $cm^{-1}$. Finally, the peaks around 1550 $cm^{-1}$ are due to N—H bending and C—N stretching vibrations in the amide groups [51].

The FTIR spectra given by the scaffolds printed with PL127-based inks, with and without SF, are shown in Fig. 4A. The peaks generated by the C—H stretching on the polymer chain are visible at 2900–3000 $cm^{-1}$ [52]. The C—O stretching vibrations of the EO and PO blocks can be observed in the 1100–1300 $cm^{-1}$ range. The PO block also shows a characteristic peak at about 900 $cm^{-1}$, corresponding to the vibration of the PO group [32,53]. The lack of peaks attributed to the amide groups of SF can be rationalized based on its low concentration in the gel. The absence of significant shifts in the positions of the peaks on the FTIR spectra of gelatin or PL127 scaffolds following the addition of SF suggests the lack of interactions between PL127 and the other polymers in the mixture. However, these interactions could also be masked by the prevalence of gelatin on PL127 in the gel.

SEM is routinely relied upon to gain insights into the structure and morphology of hydrogels [54]. SEM images of the scaffolds printed with gelatin- or PL127-based inks with different concentrations of SF are shown in Fig. 5. In both gelatin-based (Fig. 5A) and PL127-based inks (Fig. 5B), the scaffolds are characterized by a porous network where interconnected fibers or filaments can be identified, in which the fibers appear to be randomly oriented. The surface of the scaffolds appears rough, with pores of different sizes and shapes. Several parameters can affect the porosity and the pore size of 3D printed scaffolds;[2] in our case, changing the SF concentration in the ink resulted in changes to the scaffold structure . The addition of SF had a modest effect on the porosity of the gelatin-containing scaffolds, but it considerably reduced the pore size. The diameter of the fibers is also affected by the presence of SF, although not in a concentration-dependent manner (Figure S6) [55]. PL127-containing scaffolds show a higher degree of porosity as a result of the addition of SF (Figure S7), although not in a concentration-dependent manner, and a reduction in pore size. The

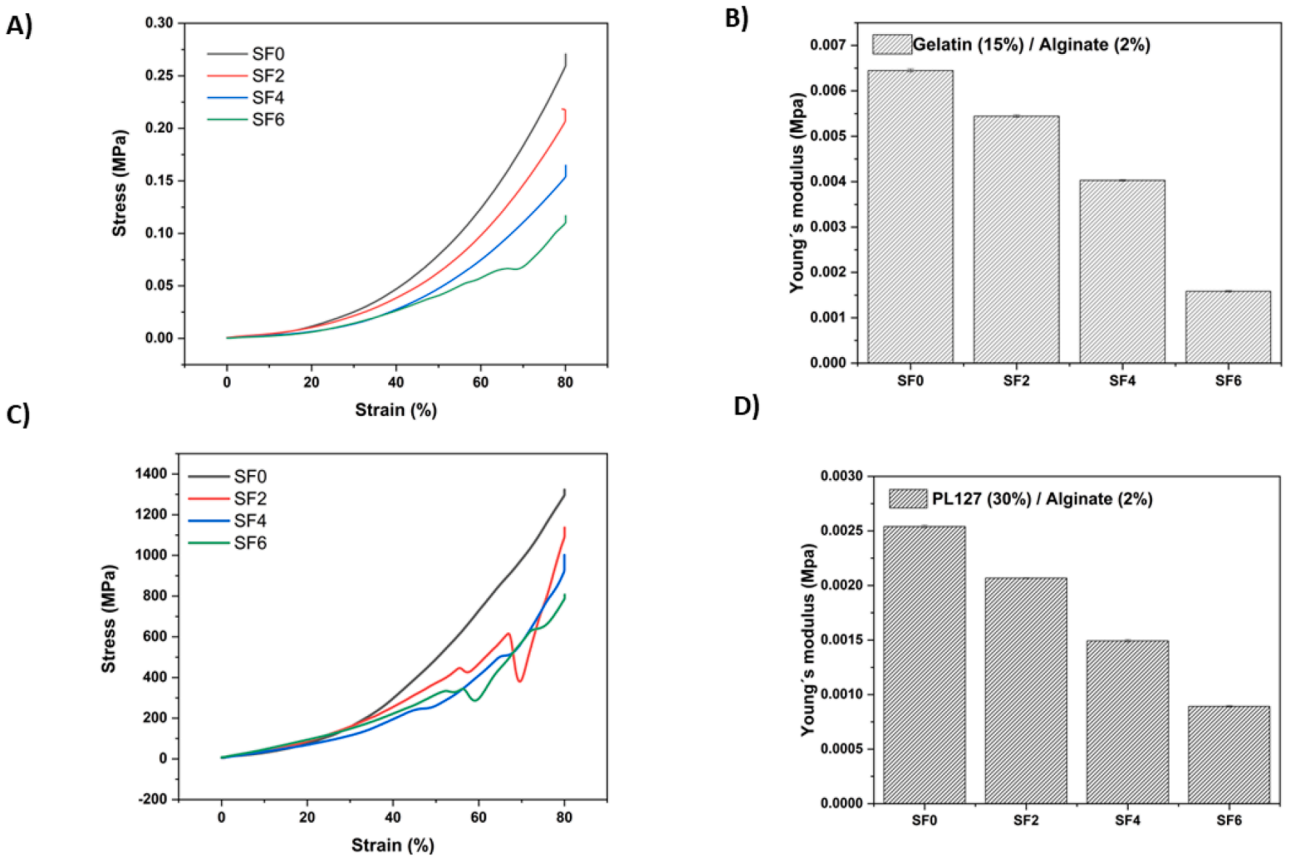


**Fig. 6.** Compression analysis of 3D printed scaffolds with varying silk fibroin concentrations: A) Strain/stress curve for gelatin-based scaffolds; B) Young's modulus for gelatin-based scaffolds; C) Strain/stress curve for PL127-based scaffolds; D) Young's modulus for PL127-based scaffolds.

presence of SF does not cause any alteration to the diameter of the fibers.

### 3.5. Compression analysis

A compression test involves applying a force to the sample and measuring the resulting deformation or displacement. The force-displacement data obtained from the test can be used to calculate parameters such as compressive strength, compressive modulus, and strain at failure [20]. This is important because it allows for predicting the printed object's behavior during handling and use. The higher the compressive strength, the more resistant the scaffold is to compression, and this parameter is determined by the printing parameters, the composition of the gel, the printing pattern, and the post-printing treatment [56].

Adding silk fibroin to both gelatin- and PL127-containing inks decreases the compression force of the printed scaffolds and results in lower Young's modulus (Fig. 6). The addition of SF can affect the gelation process of gelatin due to its ability to form hydrogen bonds with water

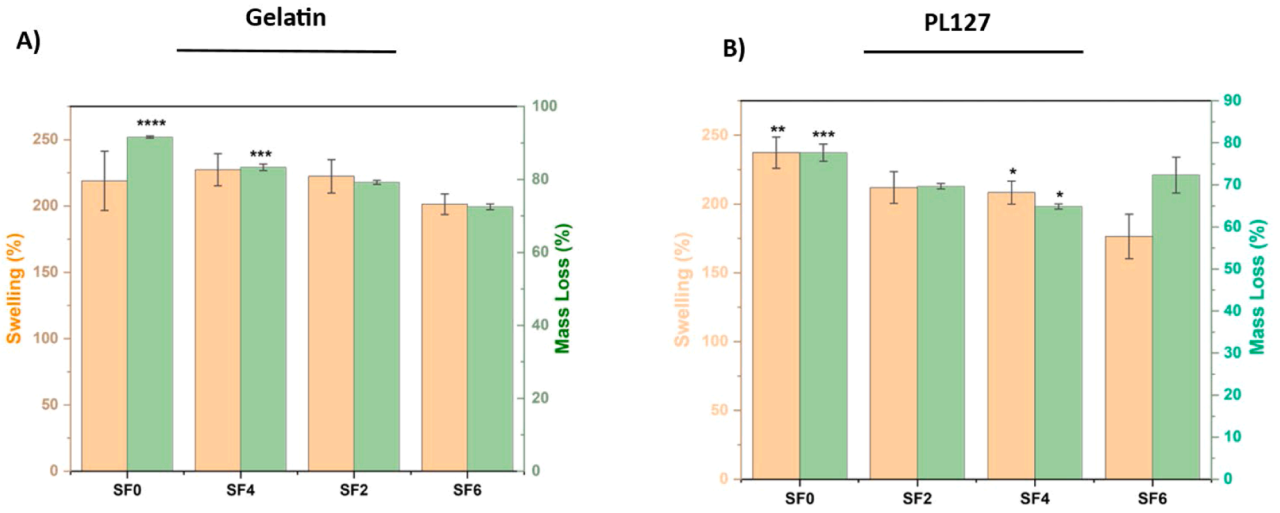


**Fig. 7.** 3D printed scaffolds swelling (orange bars) and mass loss (green bars) analysis: A) Gelatin-based scaffolds; B) PL127-based scaffolds. (*) p-value $< 0.05$, (**) p-value $< 0.01$, and (***) p-value $< 0.001$.

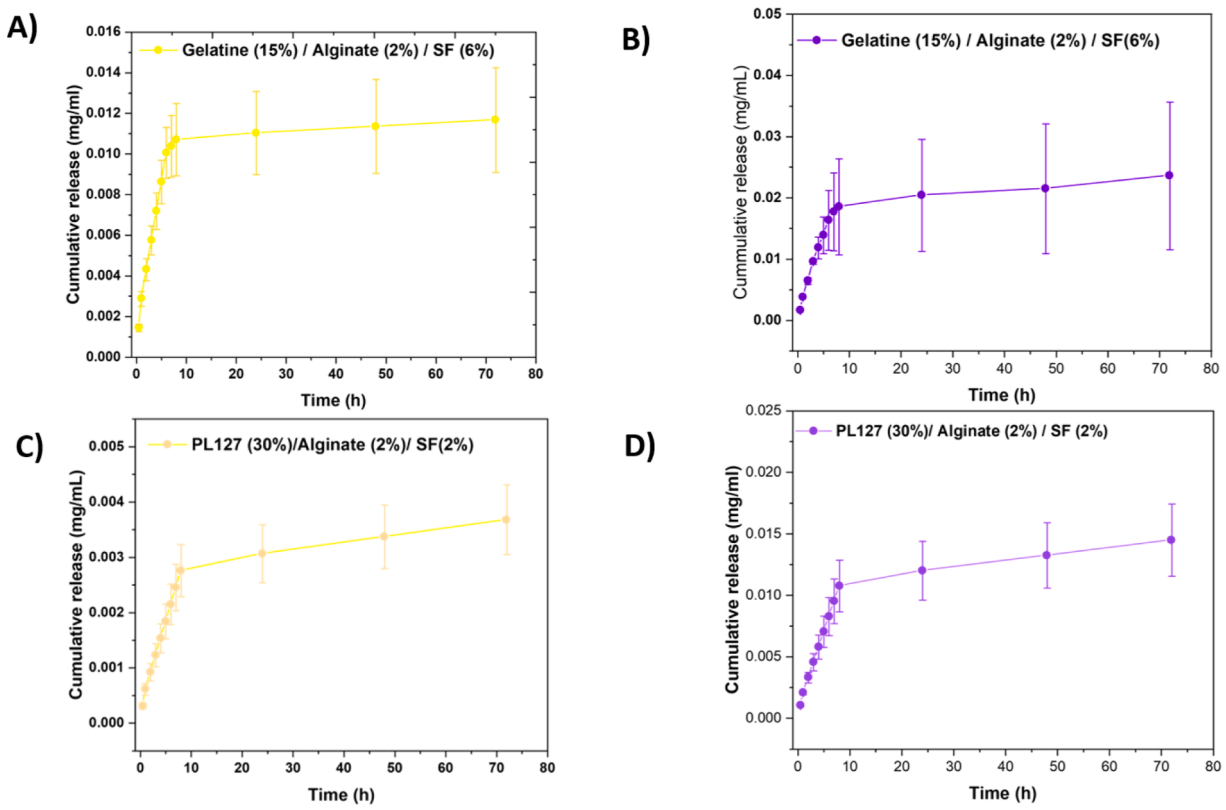


**Fig. 8.** Photosensitizers release from gelatin- and PL127-based scaffold in PBS at 0.5, 1, 2, 3, 4, 5, 6, 7, 8, 24, 48, and 72 h: A) Phenalenone released from gelatin-containing scaffold (6 % SF); B) Porphyrin released from gelatin-containing scaffold (6 % SF); C) Phenalenone released from PL127-based scaffold (2 % SF); D) Porphyrin released from PL127-based scaffold (2 % SF).

molecules. Silk fibroin has a high affinity for water, and this can cause water to be drawn away from the gelatin, leading to a delay or inhibition of the gelation process [57]. This effect can be controlled by adjusting the ratio of silk fibroin to gelatin and/or the processing conditions, such as the temperature and time of gelation. The same behavior can be observed in the scaffolds containing PL127. With the formulations used in this study, exposing the printed scaffolds to a solution containing calcium ions is critical for cross-linking the hydrogel and obtaining a scaffold for handling. The decrease in Young's modulus could be due to SF delaying the diffusion of calcium chloride through the structure, interfering with the gelation process of the hydrogel (Fig. 6B).

### 3.6. 3D hydrogels swelling and loss mass analysis

Hydrogels are three-dimensional networks of hydrophilic polymers that absorb and retain large amounts of water. The swelling behavior of hydrogels can be described by their swelling ratio, which is defined as the ratio of the swollen volume to the dry volume [58]. The swelling properties of 3D-printed hydrogels can be optimized by carefully controlling the material composition, printing parameters, and post-processing conditions [59]. This can help ensure that the hydrogel retains its ability to absorb water and maintain its structural integrity, which is critical for most biomedical applications.[47] For example, alginate hydrogels have high swelling ratios and can absorb up to several hundred times their weight in water [60]. Gelatin and silk fibroin hydrogels, on the other hand, have lower swelling ratios but can be modified to have tunable mechanical properties [61].

The presence of SF affects the swelling ratio and mass loss of the 3D-printed scaffolds obtained from gelatin-based inks (Fig. 7A). The swelling behavior of the hydrogels decreases slightly but significantly with the addition of silk fibroin, which could be attributed to a higher extent of cross-linking in the structure [60]. Hydrogels with a high crosslink density usually present a lower swelling ratio than soft cross-linked hydrogels due to the lower diffusion of the water through the structure [62]. A similar behavior is observed with scaffolds obtained by printing PL127-based inks, for which the swelling ratio decreases with increasing SF concentration. For both gel series, the degradation of the scaffolds decreases with an increase in SF concentrations within the structure due to the low degradability and solubility of the fibroin, compared with the other components of the 3D scaffolds (Fig. 7). This indicates that the presence of SF enhances mechanical properties, increasing scaffold stiffness and stability. This improvement is linked to higher cross-linking density, which strengthens the structure and reduces swelling and degradation [63].

### 3.7. Photosensitizer release analysis

To evaluate the potential of the scaffold to act as a drug reservoir for photodynamic therapy, we investigated the release of two photosensitizers from the 3D-printed hydrogels. The release profile of a drug from a hydrogel is dictated by the properties of the hydrogel (i.e., porosity, stiffness, and swelling behavior) and the aqueous solubility of the drug. For example, hydrogels with higher porosity, swelling, and degradation rate display a faster release because they facilitate the diffusion of the drug through the matrix [64]. On the other hand, the release of the drug from a stiffer hydrogel may be hampered by reduced swelling and increased resistance to drug diffusion [65]. For our study, we selected a water-soluble porphyrin (5,10,15,20-tetrakis(4-sulfonatophenyl) porphyrin tetrasodium salt) and a phenalenone as model photosensitizers due to their favorable singlet oxygen quantum yields and their used in different applications as antibacterial and wound healing [66–69]. These experiments were performed on a gelatin-based scaffold containing 6 % SF and a PL127-based scaffold containing 2 % SF due to their favorable printability and mechanical properties.

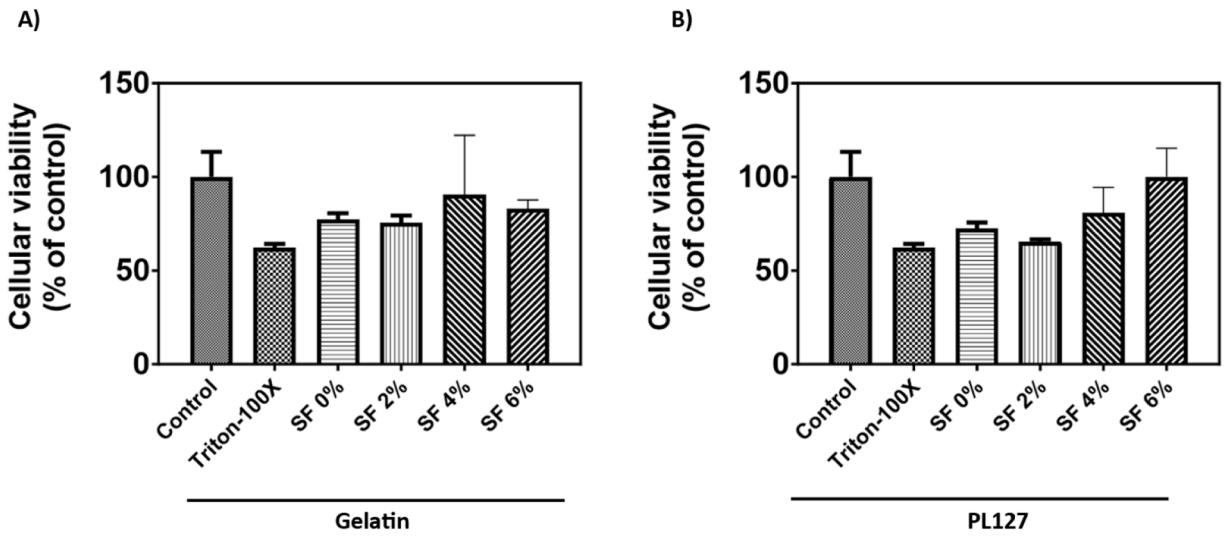


**Fig. 9.** Viability of HaCat keratinocytes following 24-h incubation with 3D printed scaffolds (MTT assay): A) Gelatin-based scaffolds; B) PL127-based scaffolds.

Fig. 8 shows the release profile of both species from the scaffolds. For both gelatin- and PL127-containing scaffolds, the release starts promptly (30 min) and reaches a plateau after a few hours. There is no significant difference between the efficiency of release of the two scaffold matrices. For the phenalenone, more efficient release seems to occur from gelatin-based scaffolds compared to PL127 scaffolds, whereas no statistically significant difference of release efficiency is shown for the porphyrin.

The variability in drug release between samples is primarily due to the progressive and non-uniform degradation of the hydrogel scaffolds upon immersion in PBS. This degradation alters the available surface area for drug diffusion, leading to inconsistencies in release kinetics [70]. Additionally, differences in hydrogel swelling behavior, influenced by polymer crosslinking and environmental factors, further impact drug diffusion rates. Non-uniform drug distribution within the hydrogel matrix also contributes to variations, as localized concentration gradients can cause some samples to release the drug faster than others [71]. Mechanical factors, such as fluid dynamics and agitation differences, further exacerbate these inconsistencies by affecting how the drug diffuses into the release medium [72].

To better characterize the release profile of the photosensitisers from the printed scaffolds, we attempted to fit our data into different drug-release models (Table S3). These mathematical models describe the release of drug molecules from different drug delivery systems, including 3D-printed scaffolds and hydrogels, and they are instrumental in helping predict the release profile of a therapeutic agent and develop new drug delivery systems [73].

The different drug release models are based on different assumptions and mathematical principles. For this study, we chose the five models most commonly adopted to describe the release of a drug from a hydrogel structure [74]. We selected a zero-order model, which assumes that drug release occurs at a constant rate, regardless of the drug concentration [75], and a first-order release model, which assumes that drug release occurs at a rate proportional to the amount of drug remaining in the drug delivery system [73]. The third model we used is the Higuchi model, which is based on the assumption that drug release occurs by diffusion through a matrix and that the process rate is proportional to the square root of time [76]. The fourth model we chose is the Korsmeyer-Peppas model, which is particularly useful for describing the drug release rate from a polymeric matrix and assumes that the drug release rate is proportional to the fractional power of time [77,78]. Lastly, the Hixson-Crowell cube root law, also known as the Hixson model, is a widely used treatment that assumes that the rate of drug release from a solid matrix is proportional to the surface area of the matrix and the difference in drug concentration between the matrix surface and the bulk of the matrix [79].

The release from the PL127-based scaffolds was best characterized by the Higuchi model, indicating that the drug release mechanism through the hydrogel occurs via Fickian diffusion. Conversely, the release from the gelatin-based scaffold was more accurately modeled by the first-order kinetics, where the release rate depends on the drug concentration within the matrix.

### 3.8. *Cell viability*

Any device intended for human, or animal use must exhibit low cytotoxicity or cytotoxicity levels deemed acceptable considering the intended application. According to ISO 10993-5 regulations, materials with cell viability percentages exceeding 80 % are classified as non-cytotoxic, those with viability between 80 % and 60 % are considered weakly cytotoxic, and viability below 40 % indicates materials with moderate or potent cytotoxicity. Resazurin viability assay performed on HaCaT keratinocytes following 24-hour incubation with the scaffolds showed at most weak cytotoxicity, compared to Triton-100X, a cell death control, indicating that the scaffold components are compatible with cell survival and suitable for use as drug reservoirs (Fig. 9).

## 4. Conclusions

This study aimed to study the potential of hydrogels as inks for the bioprinting of photosensitizers reservoirs for photodynamic therapy. We studied eight hydrogel formulations containing either gelatin or PL127 as the main component and varying concentrations of silk fibroin (from 0 % to 6 %). The printability of the hydrogels was determined by the nature of the main hydrogel component. Still, the addition of silk fibroin significantly impacts the rheological properties of the ink and the structural and mechanical features of the printed scaffold (e.g., compressive strength, porosity, etc.). Two model photosensitisers were easily incorporated in the ink formulation, and their release from the printed scaffold was already taking place after 30 min. Although the release of the drugs follows different kinetics (the Higuchi model described better the release of the photosensitisers from gelatin-based scaffolds, whereas the first-order model was better suited for the release from PL127-based scaffolds), all scaffolds display favorable swelling/degradation properties for the delivery of photosensitisers. This, together with good compatibility with cell viability, encourages further research toward applying these materials as reservoirs of therapeutic agents for photodynamic therapy.

## CRediT authorship contribution statement

**Jose Eduardo U. Rojas:** Writing – review & editing, Writing – original draft, Methodology, Investigation, Formal analysis, Data curation, Conceptualization. **Lídia Maria de Andrade:** Writing – review & editing, Supervision, Methodology, Investigation, Formal analysis, Data curation, Conceptualization. **Wendel A. Alves:** Writing – review & editing, Writing – original draft, Supervision, Project administration, Methodology, Investigation, Funding acquisition, Data curation, Conceptualization. **Francesca Giuntini:** Writing – review & editing, Writing – original draft, Supervision, Project administration, Methodology, Investigation, Funding acquisition, Data curation, Conceptualization.

## Declaration of competing interest

The authors declare that they have no known competing financial interests or personal relationships that could have appeared to influence the work reported in this paper.

## Acknowledgments

This work was supported by FAPESP (grant 2022/14753-0), CNPq grant (305574/2023-0), the National Institute of Science and Technology in Bioanalytics-INCTBio (FAPESP grant 2014/50867-3 and CNPq grant 465389/2014-7) and the Royal Society of Chemistry Research Enablement grant (E21-8697639449). J.E.U.R. is grateful for a doctoral fellowship to CAPES (project number 88882.451559/2019-01). L.M.A. thanks FAPEMIG grant (Rede Mineira de Nanomedicina Theranostica RED-00079-22) and Laboratory of Gamma Irradiation (CDTN-CNEN). The staff at LNNano are gratefully recognized for their invaluable help and access to the SEM facilities. The authors are grateful to the Multiuser Central Facilities at UFABC.

## Supplementary materials

Supplementary material associated with this article can be found, in the online version, at doi:10.1016/j.mtla.2025.102402.

## References

[1] P.A. Barbugli, C.P. Alves, E.M. Espreafico, A.C. Tedesco, Photodynamic therapy utilizing liposomal CLALPc in human melanoma 3D cell cultures, Exp. Dermatol. 24 (2015) 970–972, https://doi.org/10.1111/exd.12815.
[2] J.E.U. Rojas, B.B. Gerbelli, A.O. Ribeiro, I.L. Nantes-Cardoso, F. Giuntini, W. A. Alves, Silk fibroin hydrogels for potential applications in photodynamic therapy, Biopolymers 110 (2019) e23245, https://doi.org/10.1002/bip.23245.
[3] Satrialdi, R. Munechika, V. Biju, Y. Takano, H. Harashima, Y. Yamada, The optimization of cancer photodynamic therapy by utilization of a pi-extended porphyrin-type photosensitizer in combination with MITO-Porter, Chem. Commun. 56 (2020) 1145–1148, https://doi.org/10.1039/c9cc08563g.
[4] G. Ioele, M. De Luca, A. Garofalo, G. Ragno, Photosensitive drugs: a review on their photoprotection by liposomes and cyclodextrins, Drug Deliv. 24 (2017) 33–44, https://doi.org/10.1080/10717544.2017.1386733.
[5] H. Chen, L. Xiao, Y. Anraku, P. Mi, X. Liu, H. Cabral, A. Inoue, T. Nomoto, A. Kishimura, N. Nishiyama, K. Kataoka, Polyion complex vesicles for photoinduced intracellular delivery of amphiphilic photosensitizer, J. Am. Chem. Soc. 136 (2014) 157–163, https://doi.org/10.1021/ja406992w.
[6] X. Zhao, J. Liu, J. Fan, H. Chao, X. Peng, Recent progress in photosensitizers for overcoming the challenges of photodynamic therapy: from molecular design to application, Chem. Soc. Rev. 50 (2021) 4185–4219, https://doi.org/10.1039/D0CS00173B.
[7] J.H. Correia, J.A. Rodrigues, S. Pimenta, T. Dong, Z. Yang, Photodynamic therapy review: principles, photosensitizers, applications, and future directions, Pharmaceutics 13 (2021) 1–16, https://doi.org/10.3390/pharmaceutics13091332.
[8] S. Gan, Y. Wu, X. Zhang, Z. Zheng, M. Zhang, L. Long, J. Liao, W. Chen, Recent advances in hydrogel-based phototherapy for tumor treatment, Gels 9 (2023), https://doi.org/10.3390/gels9040286.
[9] J.E. Ulloa Rojas, V.L. de Oliveira, D.R. De Araujo, G.R. Tofoli, M.M. De Oliveira, D. J. Carastan, M. Palaci, F. Giuntini, W.A. Alves, Silk fibroin/poly(vinyl Alcohol) microneedles as carriers for the delivery of singlet oxygen photosensitizers, ACS Biomater. Sci. Eng. 8 (2022) 128–139, https://doi.org/10.1021/acsbiomaterials.1c00913.
[10] Y. Li, M. Zhang, H. Han, B. Zhang, J.B. Matson, D. Chen, W. Li, Y. Wang, Peptide-based supramolecular photodynamic therapy systems: from rational molecular design to effective cancer treatment, Chem. Eng. J. 436 (2022) 135240, https://doi.org/10.1016/j.cej.2022.135240.
[11] M.C. Kearney, S. Brown, M.T.C. McCrudden, A.J. Brady, R.F. Donnelly, Potential of microneedles in enhancing delivery of photosensitising agents for photodynamic therapy, Photodiagnosis Photodyn. Ther. 11 (2014) 459–466, https://doi.org/10.1016/j.pdpdt.2014.09.003.
[12] B. Mansoori, A. Mohammadi, M. Amin Doustvandi, F. Mohammadnejad, F. Kamari, M.F. Gjerstorff, B. Baradaran, M.R. Hamblin, Photodynamic therapy for cancer: role of natural products, Photodiagnosis Photodyn. Ther. 26 (2019) 395–404, https://doi.org/10.1016/j.pdpdt.2019.04.033.
[13] J.E.U. Rojas, B.B. Gerbelli, A.O. Ribeiro, I.L. Nantes-Cardoso, F. Giuntini, W. A. Alves, Silk fibroin hydrogels for potential applications in photodynamic therapy, Biopolymers (2018), https://doi.org/10.1002/bip.23245.
[14] L. Ma, W. Dong, E. Lai, J. Wang, Silk fibroin-based scaffolds for tissue engineering, Front. Bioeng. Biotechnol. 12 (2024). https://www.frontiersin.org/journals/bioengineering-and-biotechnology/articles/10.3389/fbioe.2024.1381838.
[15] M. Li, J. You, Q. Qin, M. Liu, Y. Yang, K. Jia, Y. Zhang, Y. Zhou, A comprehensive review on silk fibroin as a persuasive biomaterial for bone tissue engineering, Int. J. Mol. Sci. 24 (2023), https://doi.org/10.3390/ijms24032660.
[16] X. Tang, W. Wu, S. Zhang, C. He, K. Fan, Y. Fan, X. Yang, J. Li, Y. Yang, J. Ling, Photodynamic hemostatic silk fibroin film with photo-controllable modulation of macrophages for bacteria-infected wound healing, Biomater. Sci. (2024), https://doi.org/10.1039/D4BM01038H.
[17] A. Gonsalves, R.A.W. Johnstone, M.M. Pereira, A.M.P. deSantAna, A.C. Serra, A. Sobral, Abilio Sobral, New procedures for the synthesis and analysis of 5,10,15,20-tetrakis(Sulphophenyl)porphyrins and derivatives through chlorosulphonation, Heterocycles (1996): n. pag. Print. Heterocycles 43 (1996) 829–838.
[18] D.N. Rockwood, R.C. Preda, T. Yücel, X. Wang, M.L. Lovett, D.L. Kaplan, Materials fabrication from Bombyx mori silk fibroin, Nat. Protoc. 6 (2011) 1612–1631, https://doi.org/10.1038/nprot.2011.379.
[19] S. Bom, R. Ribeiro, H.M. Ribeiro, C. Santos, J. Marto, On the progress of hydrogel-based 3D printing: correlating rheological properties with printing behaviour, Int. J. Pharm. 615 (2022) 121506, https://doi.org/10.1016/j.ijpharm.2022.121506.
[20] S.H. Kim, H. Hong, O. Ajiteru, M.T. Sultan, Y.J. Lee, J.S. Lee, O.J. Lee, H. Lee, H. S. Park, K.Y. Choi, J.S. Lee, H.W. Ju, I.S. Hong, C.H. Park, 3D bioprinted silk fibroin hydrogels for tissue engineering, Nat. Protoc. 16 (2021) 5484–5532, https://doi.org/10.1038/s41596-021-00622-1.
[21] M. Gholipourmalekabadi, S. Sapru, A. Samadikuchaksaraei, R.L. Reis, D.L. Kaplan, S.C. Kundu, Silk fibroin for skin injury repair: where do things stand? Adv. Drug Deliv. Rev. 153 (2020) 28–53, https://doi.org/10.1016/j.addr.2019.09.003.
[22] A. Bucciarelli, A. Motta, Use of Bombyx mori silk fibroin in tissue engineering: from cocoons to medical devices, challenges, and future perspectives, Biomater. Adv. 139 (2022) 212982, https://doi.org/10.1016/j.bioadv.2022.212982.
[23] M.K. DeBari, M.N. Keyser, M.A. Bai, R.D. Abbott, 3D printing with silk: considerations and applications, Connect. Tissue Res. 61 (2020) 163–173, https://doi.org/10.1080/03008207.2018.1553959.
[24] Y. Nashchekina, A. Militsina, V. Elokhovskiy, E. Ivan'kova, A. Nashchekin, A. Kamalov, V. Yudin, Precisely printable silk fibroin/carboxymethyl cellulose/alginate bioink for 3D printing, Polymers 16 (2024), https://doi.org/10.3390/polym16081027.
[25] R.R. Jose, J.E. Brown, K.E. Polido, F.G. Omenetto, D.L. Kaplan, Polyol-silk bioink formulations as two-part room-temperature curable materials for 3D printing, ACS Biomater. Sci. Eng 1 (2015) 780–788, https://doi.org/10.1021/acsbiomaterials.5b00160.
[26] W. Pudkon, C. Laomeephol, S. Damrongsakkul, S. Kanokpanont, J. Ratanavaraporn, Comparative study of silk fibroin-based hydrogels and their potential as material for 3-dimensional (3D) printing, Molecules 26 (2021), https://doi.org/10.3390/molecules26133887.
[27] Q. Dou, A.A. Karim, X.J. Loh, Modification of thermal and mechanical properties of PEG-PPG-PEG copolymer (F127) with MA-POSS, Polymers 8 (2016), https://doi.org/10.3390/polym8090341.
[28] S. Chatterjee, P.C. leung Hui, C. wai Kan, W. Wang, Dual-responsive (pH/temperature) Pluronic F-127 hydrogel drug delivery system for textile-based transdermal therapy, Sci. Rep. 9 (2019) 1–13, https://doi.org/10.1038/s41598-019-48254-6.
[29] B. Shriky, A. Kelly, M. Isreb, M. Babenko, N. Mahmoudi, S. Rogers, O. Shebanova, T. Snow, T. Gough, Pluronic F127 thermosensitive injectable smart hydrogels for controlled drug delivery system development, J. Colloid Interface Sci. 565 (2020) 119–130, https://doi.org/10.1016/j.jcis.2019.12.096.
[30] N. Cui, C.Y. Dai, X. Mao, X. Lv, Y. Gu, E.S. Lee, H.B. Jiang, Y. Sun, Poloxamer-based scaffolds for tissue engineering applications: a review, Gels 8 (2022) 1–24, https://doi.org/10.3390/gels8060360.
[31] J. Youn, J.H. Choi, S. Lee, S.W. Lee, B.K. Moon, J.E. Song, G. Khang, Pluronic f-127/silk fibroin for enhanced mechanical property and sustained release drug for tissue engineering biomaterial, Materials 14 (2021) 1–11, https://doi.org/10.3390/ma14051287.
[32] E. Gioffredi, M. Boffito, S. Calzone, S.M. Giannitelli, A. Rainer, M. Trombetta, P. Mozetic, V. Chiono, Pluronic F127 hydrogel characterization and biofabrication in cellularized constructs for tissue engineering applications, Procedia CIRP 49 (2016) 125–132, https://doi.org/10.1016/j.procir.2015.11.001.
[33] V. Kokol, Y.B. Pottathara, M. Mihelčič, L.S. Perše, Rheological properties of gelatine hydrogels affected by flow- and horizontally-induced cooling rates during

3D cryo-printing, Colloids Surf. A 616 (2021), https://doi.org/10.1016/j.colsurfa.2021.126356.
[34] Y. Mao, Z. Ding, C. Yuan, S. Ai, M. Isakov, J. Wu, T. Wang, M.L. Dunn, H.J. Qi, 3D Printed reversible shape changing components with stimuli responsive materials, Sci. Rep. 6 (2016) 1–13, https://doi.org/10.1038/srep24761.
[35] I. Donderwinkel, J.C.M. van Hest, N.R. Cameron, Bio-inks for 3D bioprinting: recent advances and future prospects, Polym. Chem. 8 (2017) 4451–4471, https://doi.org/10.1039/C7PY00826K.
[36] G. Stojkov, Z. Niyazov, F. Picchioni, R.K. Bose, Relationship between structure and rheology of hydrogels for various applications, Gels 7 (2021), https://doi.org/10.3390/gels7040255.
[37] F.J. Rubio-Hernández, A.I. Gómez-Merino, C. del Pino, L. Parras, L. Campo-Deaño, F.J. Galindo-Rosales, J.F. Velázquez-Navarro, Perspectives in Fundamental and Applied Rheology, 2013.
[38] J. Xie, Y.C. Jin, Parameter determination for the cross rheology equation and its application to modeling non-Newtonian flows using the WC-MPS method, Eng. Appl. Comput. Fluid Mech. 10 (2016) 111–129, https://doi.org/10.1080/19942060.2015.1104267.
[39] J.E.U. Rojas, B.B. Gerbelli, A.O. Ribeiro, I.L. Nantes-Cardoso, F. Giuntini, W. A. Alves, Silk fibroin hydrogels for potential applications in photodynamic therapy, Biopolymers 110 (2019) e23245, https://doi.org/10.1002/bip.23245.
[40] M.Y. Yeh, J.Y. Zhao, Y.R. Hsieh, J.H. Lin, F.Y. Chen, R.D. Chakravarthy, P. C. Chung, H.C. Lin, S.C. Hung, Reverse thermo-responsive hydrogels prepared from Pluronic F127 and gelatin composite materials, RSC Adv. 7 (2017) 21252–21257, https://doi.org/10.1039/c7ra01118k.
[41] A. Basu, J. Lindh, E. Ålander, M. Strømme, N. Ferraz, On the use of ion-crosslinked nanocellulose hydrogels for wound healing solutions: physicochemical properties and application-oriented biocompatibility studies, Carbohydr. Polym. 174 (2017) 299–308, https://doi.org/10.1016/j.carbpol.2017.06.073.
[42] Q. Li, S. Xu, Q. Feng, Q. Dai, L. Yao, Y. Zhang, H. Gao, H. Dong, D. Chen, X. Cao, 3D printed silk-gelatin hydrogel scaffold with different porous structure and cell seeding strategy for cartilage regeneration, Bioact. Mater. 6 (2021) 3396–3410, https://doi.org/10.1016/j.bioactmat.2021.03.013.
[43] S. Naghieh, X. Chen, Printability–A key issue in extrusion-based bioprinting, J. Pharm. Anal. 11 (2021) 564–579, https://doi.org/10.1016/j.jpha.2021.02.001.
[44] N. Ashammakhi, S. Ahadian, C. Xu, H. Montazerian, H. Ko, R. Nasiri, N. Barros, A. Khademhosseini, Bioinks and bioprinting technologies to make heterogeneous and biomimetic tissue constructs, Mater. Today Bio 1 (2019), https://doi.org/10.1016/j.mtbio.2019.100008.
[45] Y. Wang, X. Yuan, B. Yao, S. Zhu, P. Zhu, S. Huang, Tailoring bioinks of extrusion-based bioprinting for cutaneous wound healing, Bioact. Mater. 17 (2022) 178–194, https://doi.org/10.1016/j.bioactmat.2022.01.024.
[46] Z. Gu, J. Fu, H. Lin, Y. He, Development of 3D bioprinting: from printing methods to biomedical applications, Asian J. Pharm. Sci. 15 (2020) 529–557, https://doi.org/10.1016/j.ajps.2019.11.003.
[47] D. Trucco, A. Sharma, C. Manferdini, E. Gabusi, M. Petretta, G. Desando, L. Ricotti, J. Chakraborty, S. Ghosh, G. Lisignoli, Modeling and fabrication of silk fibroin–Gelatin-based constructs using extrusion-based three-dimensional bioprinting, ACS Biomater. Sci. Eng. 7 (2021) 3306–3320, https://doi.org/10.1021/acsbiomaterials.1c00410.
[48] M.P. Das, S.P. R, K. Prasad, V. Jv, R. M, Extraction and characterization of gelatin: a functional biopolymer, Int. J. Pharm. Pharm. Sci. 9 (2017) 239, https://doi.org/10.22159/ijpps.2017v9i9.17618.
[49] Z. Peng, Z. Li, Y. Shen, Influence of chemical cross-linking on properties of gelatin/chitosan microspheres, Polym. Plast. Technol. Eng. 51 (2012) 381–385, https://doi.org/10.1080/03602559.2011.639830.
[50] W. Yu, G. Jiang, D. Liu, L. Li, H. Chen, Y. Liu, Q. Huang, Z. Tong, J. Yao, X. Kong, Fabrication of biodegradable composite microneedles based on calcium sulfate and gelatin for transdermal delivery of insulin, Mater. Sci. Eng. C 71 (2017) 725–734, https://doi.org/10.1016/j.msec.2016.10.063.
[51] F. Polyak, G. Reich, Infrared spectroscopic study of the coil-helix transition of highly concentrated gelatin formulations, Eur. J. Pharm. Biopharm. 140 (2019) 11–19, https://doi.org/10.1016/j.ejpb.2019.04.010.
[52] S. Fu, H. Yu, Redox-Sensitive Pluronic F127-Tocopherol Micelles : Synthesis, Characterization, and Cytotoxicity Evaluation, 2017, pp. 2635–2644.
[53] S. ul Hassan, I. Khalid, L. Hussain, K. Barkat, I.U. Khan, Development and evaluation of pH-responsive pluronic F 127 Co-poly- (Acrylic Acid) biodegradable nanogels for topical delivery of terbinafine HCL, Dose-Response 20 (2022) 1–13, https://doi.org/10.1177/15593258221095977.
[54] K.-C. Chang, D.-J. Lin, Y.-R. Wu, C.-W. Chang, C.-H. Chen, C.-L. Ko, W.-C. Chen, Characterization of genipin-crosslinked gelatin/hyaluronic acid-based hydrogel membranes and loaded with hinokitiol: in vitro evaluation of antibacterial activity and biocompatibility, Mater. Sci. Eng. C 105 (2019) 110074, https://doi.org/10.1016/j.msec.2019.110074.
[55] M. Sun, X. Sun, Z. Wang, S. Guo, G. Yu, H. Yang, Synthesis and properties of gelatin methacryloyl (GelMA) hydrogels and their recent applications in load-bearing tissue, Polymers 10 (2018), https://doi.org/10.3390/POLYM10111290.
[56] L. Wei, S. Wu, M. Kuss, X. Jiang, R. Sun, P. Reid, X. Qin, B. Duan, 3D printing of silk fibroin-based hybrid scaffold treated with platelet rich plasma for bone tissue engineering, Bioact. Mater. 4 (2019) 256–260, https://doi.org/10.1016/j.bioactmat.2019.09.001.
[57] V. Sencadas, C. Garvey, S. Mudie, J.J.K. Kirkensgaard, G. Gouadec, S. Hauser, Electroactive properties of electrospun silk fibroin for energy harvesting applications, Nano Energy 66 (2019) 104106, https://doi.org/10.1016/j.nanoen.2019.104106.
[58] H.Y. Wang, Y.Q. Zhang, Processing silk hydrogel and its applications in biomedical materials, Biotechnol. Prog. 31 (2015) 630–640, https://doi.org/10.1002/btpr.2058.
[59] S.M. Bittner, H.A. Pearce, K.J. Hogan, M.M. Smoak, J.L. Guo, A.J. Melchiorri, D. W. Scott, A.G. Mikos, Swelling behaviors of 3D printed Hydrogel and Hydrogel-microcarrier composite scaffolds, Tissue Eng. Part A 27 (2021) 665–678, https://doi.org/10.1089/ten.tea.2020.0377.
[60] S.D. Dutta, J. Hexiu, D.K. Patel, K. Ganguly, K.T. Lim, 3D-printed bioactive and biodegradable hydrogel scaffolds of alginate/gelatin/cellulose nanocrystals for tissue engineering, Int. J. Biol. Macromol. 167 (2021) 644–658, https://doi.org/10.1016/j.ijbiomac.2020.12.011.
[61] J.-P. Fan, Z.-T. Lai, D.-Y. Mao, C.-F. Xie, H.-P. Chen, H.-L. Peng, Preparation of a silk fibroin/gelatin composite hydrogel for high-selectively adsorbing bovine hemoglobin, Colloids Surf. A 660 (2023) 130869, https://doi.org/10.1016/j.colsurfa.2022.130869.
[62] R.B. Ester-bridged, G. Hoti, F. Caldera, C. Cecone, A.R. Pedrazzo, A. Anceschi, S.L. Appleton, Y.K. Monfared, F. Trotta, Effect of the cross-linking density on the swelling, (2021).
[63] Q. Niu, L. Huang, S. Fan, X. Yao, Y. Zhang, 3D Printing silk fibroin/polyacrylamide triple-network composite hydrogels with stretchability, conductivity, and strain-sensing ability as bionic electronic skins, ACS Biomater. Sci. Eng. 10 (2024) 3489–3499, https://doi.org/10.1021/acsbiomaterials.4c00201.
[64] F.M. Carbinatto, A.D. de Castro, R.C. Evangelista, B.S.F. Cury, Insights into the swelling process and drug release mechanisms from cross-linked pectin/high amylose starch matrices, Asian J. Pharm. Sci. 9 (2014) 27–34, https://doi.org/10.1016/j.ajps.2013.12.002.
[65] A.R. Abbasi, M. Sohail, M.U. Minhas, T. Khaliq, M. Kousar, S. Khan, Z. Hussain, A. Munir, Bioinspired sodium alginate based thermosensitive hydrogel membranes for accelerated wound healing, Int. J. Biol. Macromol. 155 (2020) 751–765, https://doi.org/10.1016/j.ijbiomac.2020.03.248.
[66] J. Godard, F. Brégier, P. Arnoux, B. Myrzakhmetov, Y. Champavier, C. Frochot, V. Sol, New phenalenone derivatives: synthesis and evaluation of their singlet oxygen quantum yield, ACS Omega 5 (2020) 28264–28272, https://doi.org/10.1021/acsomega.0c04172.
[67] S.R.M. Ibrahim, A.M. Omar, Y.A. Muhammad, A.A. Alqarni, A.M. Alshehri, S.G. A. Mohamed, H.M. Abdallah, M.A. Elfaky, G.A. Mohamed, J. Xiao, Advances in fungal phenaloenones-natural metabolites with great promise: biosynthesis, bioactivities, and an In silico evaluation of their potential as Human glucose transporter 1 inhibitors, Molecules 27 (2022), https://doi.org/10.3390/molecules27206797.
[68] J. Godard, D. Gibbons, S. Leroy-Lhez, R.M. Williams, N. Villandier, T.-S. Ouk, F. Brégier, V. Sol, Development of phenalenone-triazolium salt derivatives for aPDT: synthesis and antibacterial screening, Antibiotics 10 (2021), https://doi.org/10.3390/antibiotics10060626.
[69] M.C.S. Vallejo, N.M.M. Moura, A.T.P.C. Gomes, A.S.M. Joaquinito, M.A. F. Faustino, A. Almeida, I. Gonçalves, V.V. Serra, M.G.P.M.S. Neves, The role of porphyrinoid photosensitizers for skin wound healing, Int. J. Mol. Sci. 22 (2021), https://doi.org/10.3390/ijms22084121.
[70] N.F. Sczesny, H.J. Wiggers, C.Z. Bueno, P. Chevallier, F. Copes, D. Mantovani, From burst to sustained release: the effect of antibiotic structure incorporated into Chitosan-based films, Antibiot. 13 (2024), https://doi.org/10.3390/antibiotics13111055.
[71] R. Gautam, I. Matai, S. Soni, Photothermally modulated drug release kinetics for pH and thermo-responsive hydrogel system, J. Mater. Res. 39 (2024) 398–411, https://doi.org/10.1557/s43578-023-01233-0.
[72] S. Sheth, E. Barnard, B. Hyatt, M. Rathinam, S.P. Zustiak, Predicting drug release from degradable hydrogels using fluorescence correlation spectroscopy and mathematical modeling, Front. Bioeng. Biotechnol 7 (2019) 1–12, https://doi.org/10.3389/fbioe.2019.00410.
[73] N.S. Heredia, K. Vizuete, M. Flores-Calero, V. Katherine Pazmiño, F. Pilaquinga, B. Kumar, A. Debut, Comparative statistical analysis of the release kinetics models for nanoprecipitated drug delivery systems based on poly(lactic-co-glycolic acid), PLoS ONE 17 (2022) 1–28, https://doi.org/10.1371/journal.pone.0264825.
[74] P. Trucillo, Drug carriers: a review on the most used mathematical models for drug release, Processes 10 (2022), https://doi.org/10.3390/pr10061094.
[75] C.G. Varelas, D.G. Dixon, C.A. Steiner, Zero-order release from biphasic polymer hydrogels, J. Control. Release 34 (1995) 185–192, https://doi.org/10.1016/0168-3659(94)00085-9.
[76] M.P. Paarakh, P.A.N.I. Jose, C.M. Setty, G.V. Peter, Release kinetics – concepts and applications, Int. J. Pharm. Res. Technol. 8 (2019) 12–20, https://doi.org/10.31838/ijprt/08.01.02.
[77] I.Y. Wu, S. Bala, N. Škalko-Basnet, M.P. di Cagno, Interpreting non-linear drug diffusion data: utilizing Korsmeyer-Peppas model to study drug release from liposomes, Eur. J. Pharm. Sci. 138 (2019) 105026, https://doi.org/10.1016/j.ejps.2019.105026.
[78] L. Ahmed, R. Atif, T.S. Eldeen, I. Yahya, A. Omara, M. Eltayeb, Study the using of nanoparticles as drug delivery system based on mathematical models for controlled release, Int. J. Latest Technol. Eng. Manag. Appl. Sci. 8 (2019) 52–56. www.ijltemas.in.
[79] A. Lisik, W. Musiał, Conductomeric evaluation of the release kinetics of active substances from pharmaceutical preparations containing iron ions, Materials 12 (2019), https://doi.org/10.3390/ma12050730.